Numerical optimization and performance analysis of lead-free titanium-based inorganic perovskite solar cells using ZnO and NiO as charge transport materials

ANCHAL SRIVASTAVA[1], R. K. SHUKLA[1], K. C. DUBEY[2,*]
[1]*Department of Physics, University of Lucknow, Lucknow-226007, India*
[2]*Department of Physics, Shia PG College, Lucknow-226020, India*

Halide-based perovskite materials offer significant advantages like high efficiency, ease of production, and cost-effectiveness. Recently, lead-free titanium-based inorganic perovskite solar cells (PSCs) have gained attention due to environmental concerns about lead. Titanium's non-toxicity, durability, and affordability make it a promising alternative. Using SCAPS-1D software, this study optimized the PSC performance by adjusting parameters such as perovskite layer thickness, defect density, and doping concentration. The optimized $CH_3NH_3SnBr_3/Cs_2TiBr_6$ PSC achieved a power conversion efficiency of 27.86%, highlighting its potential for advancing research in lead-free PSCs.

(Received August 16, 2024; accepted April 3, 2025)

Keywords: Perovskite, NiO, ZnO, Cs_2TiBr_6, $CH_3NH_3SnBr_3$

1. Introduction

Access to affordable energy sources is serious for long-term community and economic growth [1]. In today's globe, energy consumption is continually rising. According to Das et al. [2], the world is becoming increasingly industrialized, with rising living standards. The majority of energy is derived from finite and dirty fossil resources. Several sources of energy have been established to meet escalating energy demand. Solar energy is the most realistic solution in this case [3-4]. Improving solar cell efficiency can assist meet global energy demands, particularly in developing countries. Photovoltaic cells generate direct current from sun irradiation [5]. PSCs have proved to be among the most promising. It is tough to achieve a PCE of more than 25% on single junction construction. The main problem with using PSCs is device stability in the air under lighting and the toxicity of the chemicals used. The presence of toxic metals such as lead is associated with it. The whole life cycle of PSCs causes substantial environmental concerns. As a result of the next high efficiency, more research communities and industrialists are questioning its future, paving the way for lead-free perovskites. Numerous lead-free perovskite absorbers have a wide bandgap and are suitable for replacement. Further advancements in tin-based PSCs can be accomplished by optimizing a variety of parameters and device designs, which will serve as the foundation for future research [6-11]. This simulation effort was directed toward the development of a perovskite based on Cs_2TiBr_6 and methylammonium tin bromide [12-18]. The layer thickness doping levels and defect density can vary, including the ETL, absorber layer, and HTL, have been altered, and the consequences have been investigated for future development. The greatest achievable efficiency is 27.86%, the highest recorded too far.

2. Methodology

2.1. Simulation software

Simulation of solar cell device performance is essential for optimizing innovative material devices. Many software are available to simulate cell properties [19].

2.2. Mathematical modelling

The SCAPS-1D software is used by solving the Poisson's and the electron (hole) continuity equation [20,21]. This simulation project required extensive research. $Cs_2TiBr_6/CH_3NH_3SnBr_3$ is a light-absorbing compound. Unlike lead-based perovskites, it is not poisonous. $CH_3NH_3SnBr_3$ could be a good, high-contrast alternative to $CH_3NH_3PbX_3$. The simulation's configuration is the most important component. This task will do a device simulation. The cleavage configuration of $FTO/ZnO/CH_3NH_3SnBr_3/Cs_2TiBr_6/NiO/Au$ is shown in Fig. 1. Light passes through the FTO edge, and $CH_3NH_3SnBr_3/Cs_2TiBr_6$ serves as the primary light absorption layer sandwiched Fluoride-doped tin oxide (FTO) forms the front and back metal connections between ETL and HTL gold (Au). ZnO is a good ETL option for solar cells [22-27]. This study focuses on simulating configurations with various features. The thickness of the various layers is specified throughout the

simulation. Doping concentration, effective state density of the conduction band (CB), and valence band (VB) are all variables. Investigate the appropriate optical and electrical properties for achieving high PCE.

2.3. Solar cell structure

Fig. 1 shows the proposed solar cell structure: FTO/ZnO/$CH_3NH_3SnBr_3$/Cs_2TiBr_6/NiO/Au. The proposed solar cell is illuminated by the standard AM 1.5 G1 sun through an FTO layer.

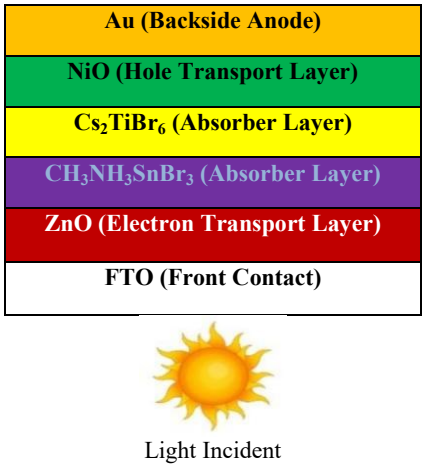

Fig. 1. Schematic structure of FTO/ZnO/$CH_3NH_3SnBr_3$/Cs_2TiBr_6/NiO/Au-based solar cell (colour online)

2.4. Photovoltaic devices have three main parts

Light absorber Charge carriers are layers that convert incident photons into electrons and holes; carrier collectors capture carriers; and metal contacts transmit them to an external circuit. The absorber used here is $CH_3NH_3SnBr_3$/Cs_2TiBr_6. The simulation was based on a number of previous research studies. These references are cited. Table 1 has the following values: Considered when creating the core configuration simulation approach to attain the best outcomes through variations.

Table 1. Physical parameters values used in the simulation

Physical Parameters	Symbol	Unit	NiO (HTL)	$CH_3NH_3SnBr_3$	Cs_2TiBr_6	ZnO (ETL)
Thickness	t	nm	150	500	400	50
Energy Band Gap	E_g	eV	3.6	1.3	1.8	3.3
Electron Affinity	X	eV	1.8	4.17	4.0	3.9
Dielectric Permittivity (Relative)	ε_r	-	11.7	10	10	9
Density of States at Valence Band	N_V	cm^{-3}	2.5×10^{20}	1.8×10^{18}	6×10^{19}	1.8×10^{19}
Density of States at Conduction Band	N_C	cm^{-3}	2.5×10^{20}	2.2×10^{18}	2×10^{19}	3.7×10^{18}
Hole Thermal Velocity	V_e	cm/s	1×10^{7}	1×10^{7}	1×10^{7}	1×10^{7}
electron Thermal Velocity	V_h	cm/s	1×10^{7}	1×10^{7}	1×10^{7}	1×10^{7}
Electron Mobility	μ_e	$cm^2/V.s$	2.8	1.6	4.4	100
Hole Mobility	μ_h	$cm^2/V.s$	2.8	1.6	2.5	25
Uniform Shallow Donor Doping	ND	cm^{-3}	0	1×10^{13}	1×10^{19}	1×10^{18}
Uniform Shallow Acceptor Doping	NA	cm^{-3}	3×10^{18}	1×10^{13}	1×10^{19}	0
Defect Density	N_t	cm^{-3}	1×10^{15}	1×10^{15}	1×10^{15}	1×10^{15}
References			28	29	30	31

3. Result and discussion

Before enhancing each factor that determines the power conversion efficiency of PSCs, the baseline parameters for the PSC device were established. These featured a 50 nm ZnO ETL layer, a 400 nm Cs_2TiBr_6 absorber layer, a 500 nm $CH_3NH_3SnBr_3$, and a 150 nm NiO HTL layer. At AM 1.5G, the device operated under continuous illumination of 1000 W/m^2 at 300 K. Table 2 displays the initial values for V_{oc}, J_{sc}, FF, and PCE.

Table 2. Solar cell initial parameters for the FTO/TiO_2/Cs_2TiBr_6/$CH_3NH_3SnBr_3$/Au PSC structure

V_{oc}	J_{sc}	FF	PCE
0.9574 V	25.11 mA/cm^2	12.17%	2.92%

Influence layer thickness of ETL (ZnO): The main role of ETL is to transmit electrons from the absorber layer to the conducting electrode and prevent them from recombining with holes [32]. As ETL thickness rises, so does series resistance, and therefore recombination occurs. We can vary the thickness of the ETL from 10 to 500 nm. Fig. 2 indicates that PV parameters are almost constant. The ETL thickness has no effect on the PV parameters, consistent with earlier research [33]. This is because ZnO has relatively large electron mobility, allowing electrons to pass through for very thin layers of ZnO. The low value of band gap also decreases the layer's resistance. The value of J_{SC} comes out at 175 nm is 25.10 mA/cm^2 and PCE equal to 2.93 %. The ETL thickness of 175 nm is taken as ideal.

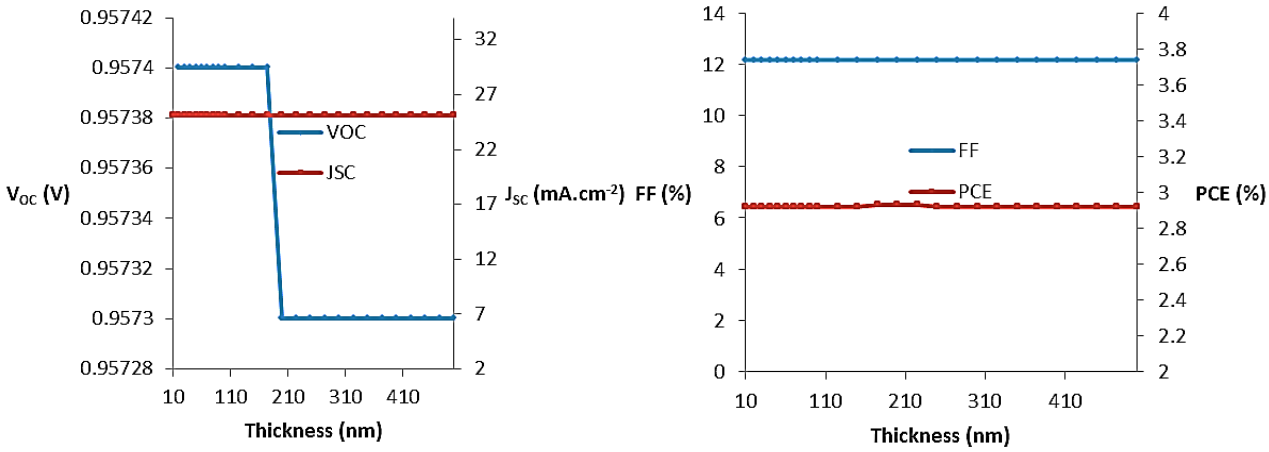

Fig. 2. Influence of ETL (ZnO) layer thickness on V_{oc}, J_{sc}, FF and PCE (colour online)

Influence of shallow donor density (N_D) of ETL (ZnO): To obtain best performance, N_D is set between 10^9 and 10^{22} cm^{-3}. Fig. 3 displays that when the value of N_D in the ZnO layer is equal to 10^{18} cm^{-3}, PCE rises from 2.86 to 2.93%. The upward trend in PCE can be attributed to higher FF from 12.10 to 12.17% at the same donor density (10^{18} cm^{-3}). J_{sc} increases from 24.74 to 25.12 mA/cm^2 when donor density rises from 10^9 to 10^{22} cm^{-3}. By adjusting N_D has no noticeable impact on V_{oc}. The rise in PCE is due to the efficient charge carrier collection and transmission and less number of charge carriers created or collected [34].

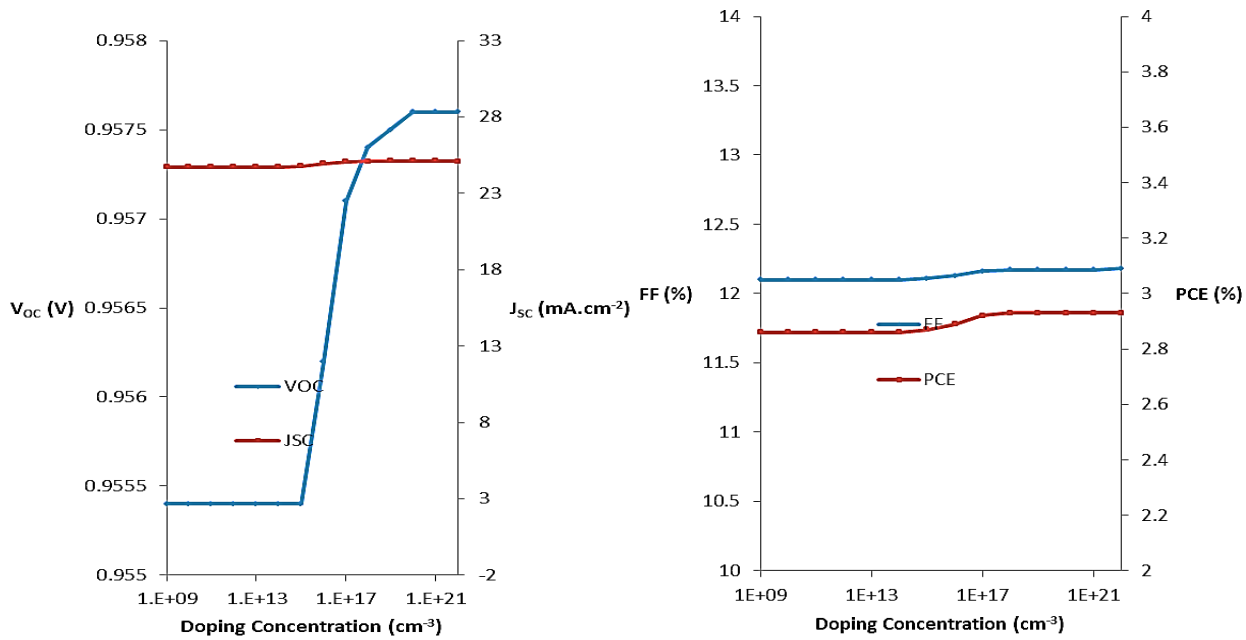

Fig. 3. Influence of shallow donor concentration of ETL layer on V_{oc}, J_{sc}, FF and PCE (colour online)

Influence of defect density (N_t) of ETL (ZnO): To improve the effectiveness of the suggested PSC design, the trap density of states (N_t) in the ZnO layer was increased from 10^9 to 10^{22} cm^{-3}. Fig. 4 illustrates how the N_t adjustment in the ETL (ZnO) impacts the photovoltaic characteristics. The graph indicates that PV parameters remain constant when N_t grows from 10^9 to 10^{22} cm^{-3}.

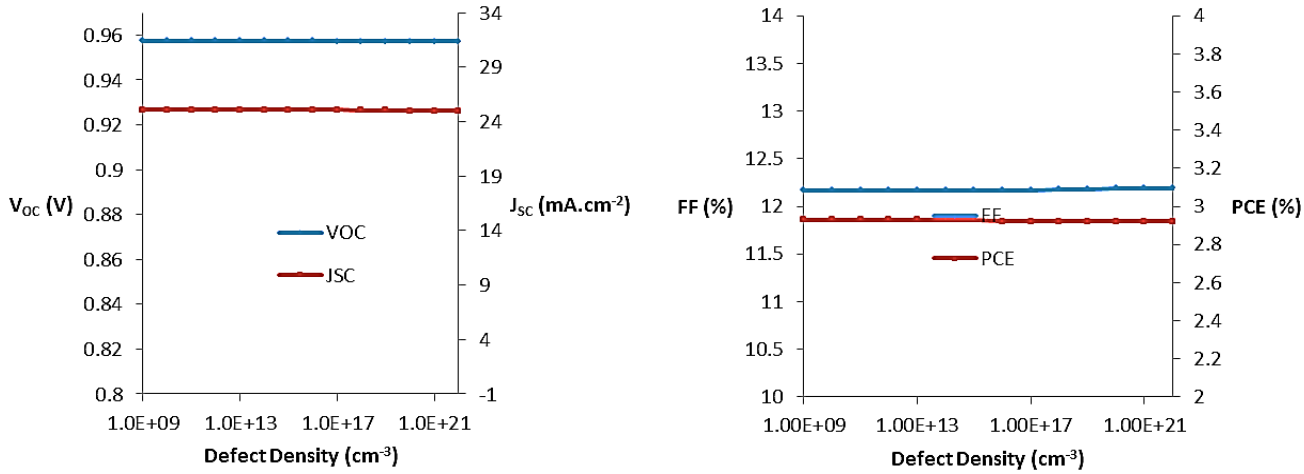

Fig. 4. Influence of N_t in ZnO layer on V_{oc}, J_{sc}, FF and PCE (colour online)

Influence of thickness of absorber layer $CH_3NH_3SnBr_3$: The thickness of the absorber layer has a considerable impact on the solar cell's performance. The absorber layer of the solar cell captures photons and transfers photo-induced hole and electron carriers to the cell's collecting electrodes [35]. For a certain thickness of the absorber layer may become saturated with photon absorption, resulting in nearly constant PV performance. The film structure has a significant impact on the durability and diffusion length of photo-generated carriers, which affects the absorber layer's performance. When the absorption layer is very thin, in this situation the resulting charge carrier can reach the electrode. If the thickness increases for a certain point, optical absorption approaches saturation. The thickness of this layer should be carefully calibrated to absorb the most protons while limiting reverse saturation current. The thickness of $CH_3NH_3SnBr_3$ was changed from 25 nm to 1500 nm. Fig. 5 shows that increasing the absorber layer thickness enhances the short circuit current density initially up to 375 nm before decreasing. The values of PV parameters fall as the layer thickness increases from 25 to 1500 nm.

The short current density value increases from 14.03 mA/cm^2 to 25.52 mA/cm^2 as layer thickness grows from 25 to 375 nm, then declines to 20.01 mA/cm^2 at 1500 nm. However, the efficiency drops from 8.35% to 2.08%, V_{oc} from 1.16 V to 0.85 V, and FF from 51.80% to 12.33%. This change is due to increased absorber thickness, results are increased recombination and saturation current [36].

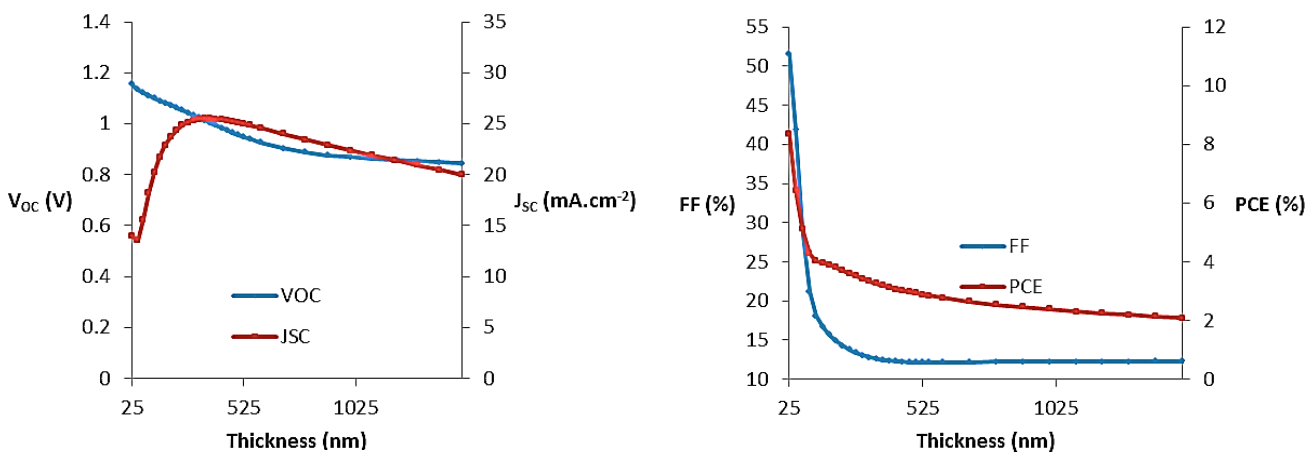

Fig. 5. Influence of absorber layer thickness of $CH_3NH_3SnBr_3$ on V_{oc}, J_{sc}, FF and PCE (colour online)

Influence of doping concentration (N_D) of absorber layer $CH_3NH_3SnBr_3$: In this study, we look at the impacts of altering the concentration of Uniform Shallow Donors in the initial absorber layer. Our experiment involves calculating various photovoltaic properties while varying the Uniform Shallow Donor concentration between 10^9 and 10^{22} cm^{-3}, with the goal of determining the optimal value for the $CH_3NH_3SnBr_3$ layer. Fig. 6 displays the results, which comprise V_{oc}, J_{sc}, fill factor and PCE. The V_{OC} value is 1.2593 V, the J_{SC} is 15.11 mA/cm^2, and the fill factor is 78.00% at 10^{22} cm^{-3}. The greatest PCE (~14.84%) is achieved at N_D equal to 10^{22} cm^{-3}. A maximum PCE (~14.84%) is achieved at a Uniform Shallow Donor concentration of 10^{22} cm^{-3} within the first absorber layer $CH_3NH_3SnBr_3$.

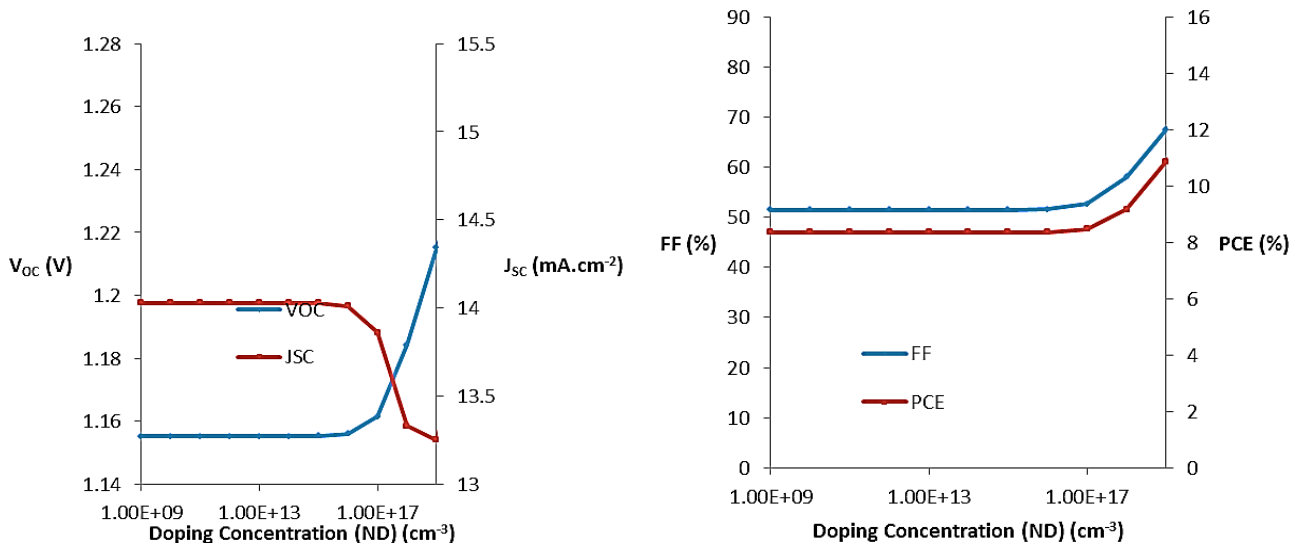

Fig. 6. V_{oc}, J_{sc}, FF and PCE of first absorber layer $CH_3NH_3SnBr_3$ as a function of Uniform Shallow Donor concentration in proposed solar cells (colour online)

Effect of doping concentration (N_A) in ($CH_3NH_3SnBr_3$) absorber layer: In this section, we look at the effect of changing the concentration of Uniform Shallow Acceptors in the first absorber layer. Our investigation involves computing photovoltaic parameters while varying the Uniform Shallow Acceptor concentration from 10^9 to 10^{22} cm^{-3}, with the goal of establishing the optimal value for the $CH_3NH_3SnBr_3$ absorber layer in the proposed solar cell. The results, which include V_{oc}, J_{sc}, FF, and PCE, are shown in Fig. 7. The maximum PCE (~14.84%) was attained at a concentration of 10^{15} cm^{-3} in the absorber layer.

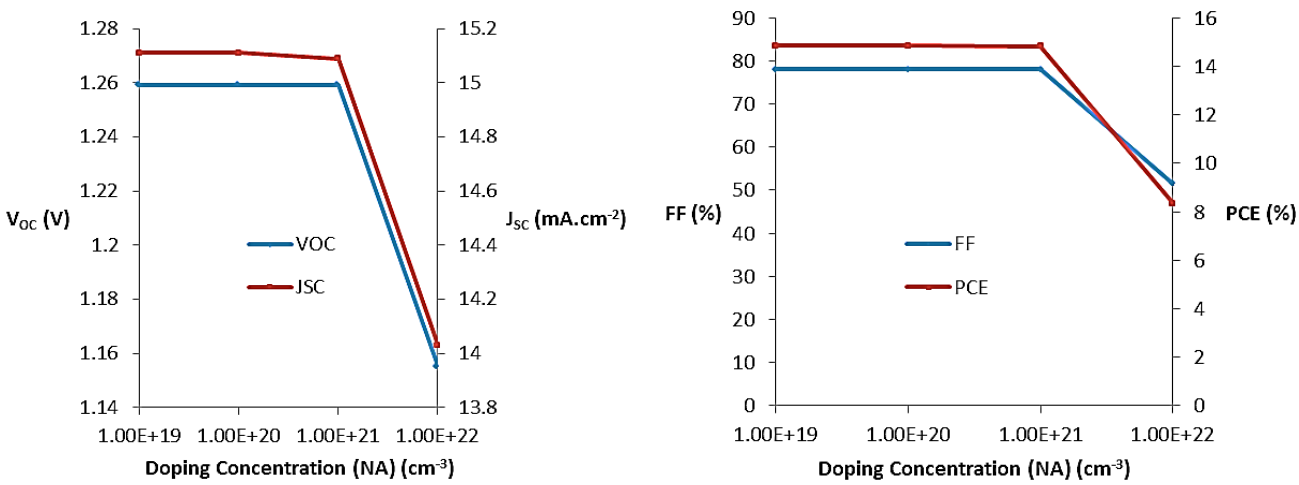

Fig. 7. V_{oc}, J_{sc}, FF and PCE of first absorber layer as a function of Uniform Shallow Acceptor Doping in $CH_3NH_3SnBr_3$ (colour online)

Influence of defect density (N_t) in $CH_3NH_3SnBr_3$: The initial N_t value for this layer is set to 10^{15} cm^{-3}. Fig. 8 illustrates the relationship between PV parameters and N_t within the absorber layer. Significant improvements in the PV properties of the PSC are observed when the N_t concentration in the perovskite decreases, which is consistent with previous findings on lead perovskites. At an N_t of 10^{10} cm^{-3}, the cell's PV properties improve dramatically, with a J_{sc} of 17.75 mA/cm^2, V_{oc} of 1.2649 V, FF of 77.70%, and PCE of 17.45%. The defect density is set to 10^{10} cm^{-3}, allowing all PV parameters to reach maximum levels.

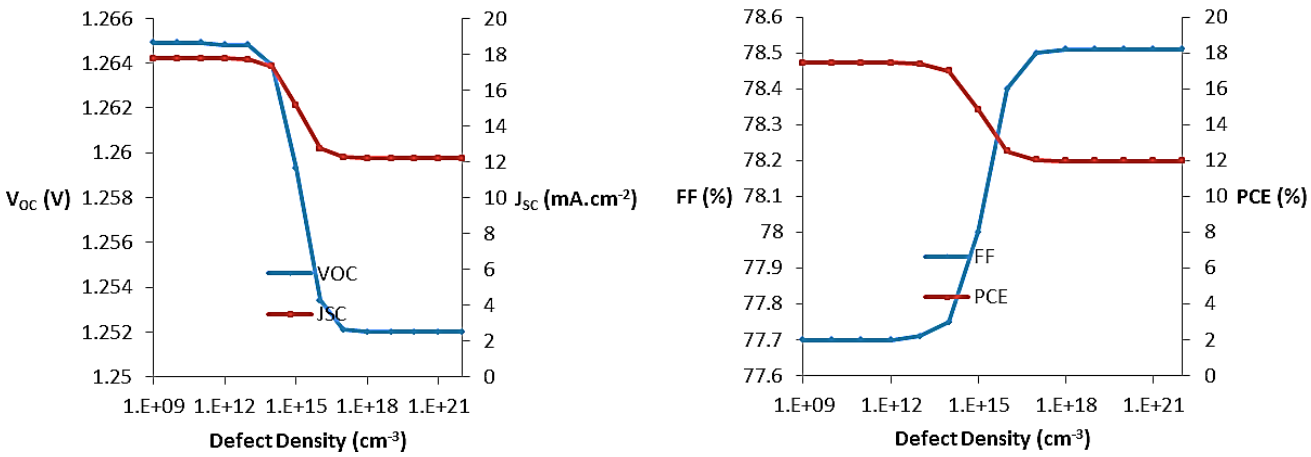

Fig. 8. Illustrates the variation of PV parameters with defect density (N_t) of first absorber layer $CH_3NH_3SnBr_3$ (colour online)

Optimal value of thickness of second layer (Cs_2TiBr_6): Similarly, the layer thickness of Cs_2TiBr_6 is changed between 400 and 1500 nm to discover the optimal thickness. Fig. 9 depicts the influence of layer thickness on solar cell performance. Fig. 9 shows that by increasing the thickness of the layer only short circuit current density increases and other parameters decrease. The J_{sc} rises from 17.75 to 20.15 mA/cm^2 as the layer width increases from 400 to 1500 nm. As the thickness increases from 400 to 1500 nm, the efficiency decreases from 17.45 to 14.49%, V_{oc} from 1.2649 to 1.1808 V and FF from 77.70 to 60.91%, respectively.

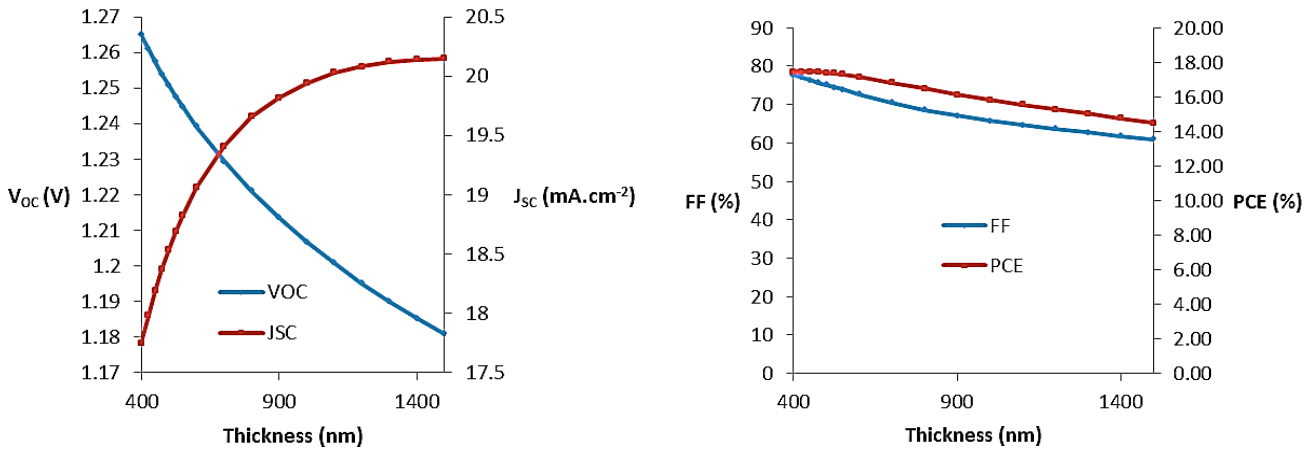

Fig. 9. Influence of absorber layer thickness on V_{oc}, J_{sc}, FF and PCE (colour online)

Influence of doping concentration (N_D) Cs_2TiBr_6 of second absorber layer: Fig. 10 shows the value of N_D in the layer (Cs_2TiBr_6) to 10^{21} results in a maximum PCE of 22.95% for the cell. As the doping concentration increases from 10^9 to 10^{22} cm^{-3}, the FF value rises from 88.90 to 91.94%. The software is then updated with the new doping concentration value for the second Layer of Cs_2TiBr_6. The N_D of the second absorber layer (Cs_2TiBr_6) is tuned to around 10^{21} cm^{-3} using photovoltaic metrics such as V_{OC}, J_{SC}, FF, and PCE, as presented in Fig. 10.

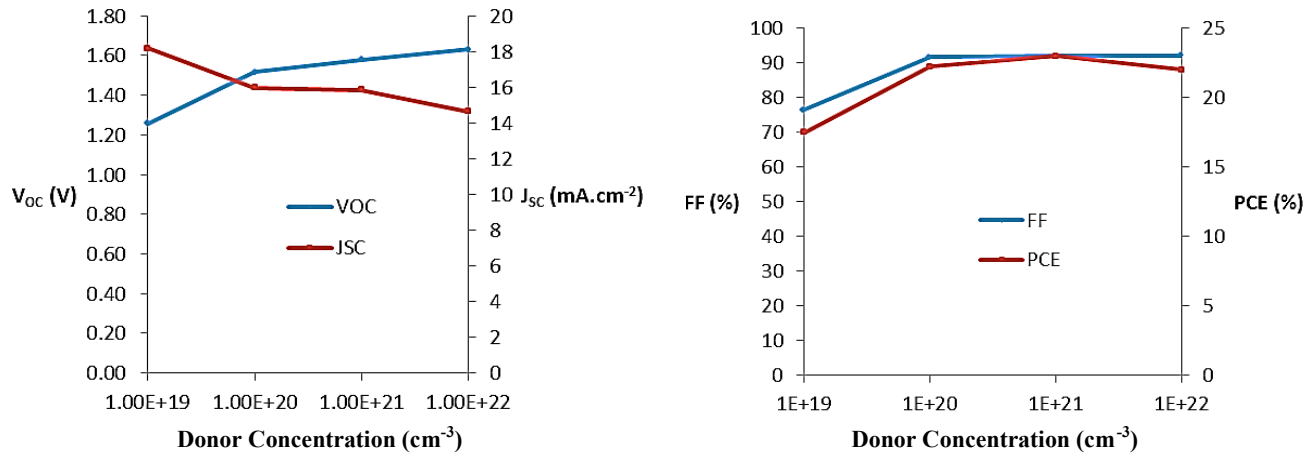

Fig. 10. V_{oc}, J_{sc}, FF and PCE of second absorber layer Cs_2TiBr_6 as a function of Uniform Shallow Donor concentration in proposed solar cell (colour online)

Effect of doping concentration (N_A) in (Cs_2TiBr_6) second Absorber Layer: In this section, we look at the impact of changing the concentration of uniform shallow acceptors in the second absorber layer. Our study involves analysing photovoltaic qualities while varying the Uniform Shallow Acceptor concentration between 10^9 and 10^{22} cm^{-3}, with the best value for the Cs_2TiBr_6 layer in the solar cell. Fig. 11 shows the results, including V_{OC}, J_{SC}, FF, and PCE. The graphic depicts how adjusting the Uniform Shallow Acceptor concentration impacts photovoltaic metrics such as V_{OC}, J_{SC} and FF. The highest PCE (~25.48%) was recorded at a concentration of 10^{22} cm^{-3} in this layer.

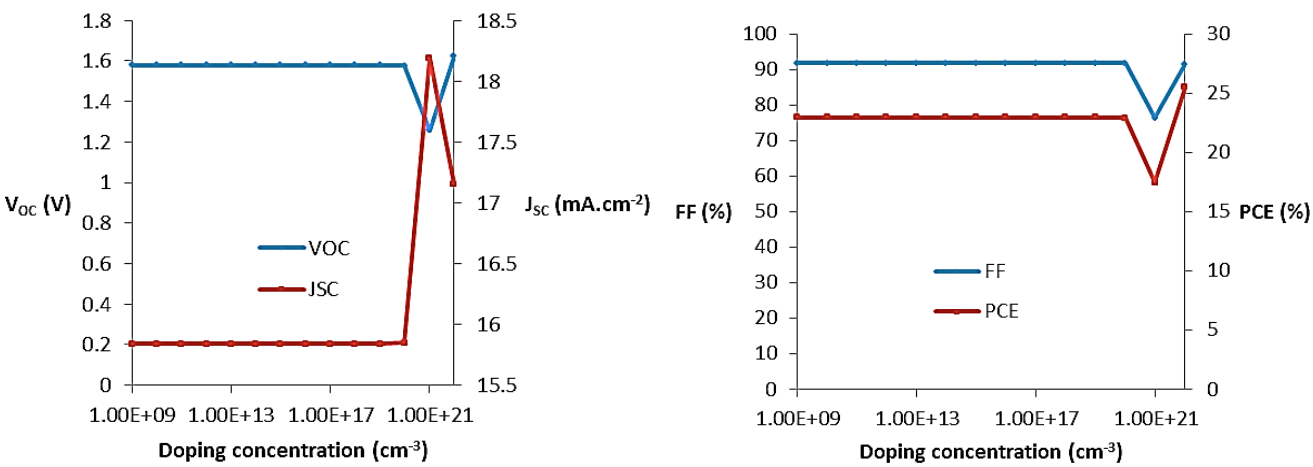

Fig. 11. V_{oc}, J_{sc}, FF and PCE of second absorber layer as a function of Uniform Shallow Acceptor concentration in Cs_2TiBr_6 (colour online)

Influence of defect density (N_t) in Cs_2TiBr_6: The initial N_t value in the second absorber layer is 10^{15} cm^{-3}. Fig. 12 shows the relationship between PV parameters and N_t in the second absorber layer. Significant improvements in the PV properties of the PSC occur as the N_t content of the perovskite is reduced, which is consistent with previous studies on lead perovskites. At a defect density of 10^{11} cm^{-3}, the cell's PV characteristics increase dramatically, with a J_{sc} of 18.22 mA/cm^2, V_{oc} of 1.6635 V, FF of 91.93%, and PCE of 27.86%. The N_t is optimized to 10^{15} cm^{-3}, allowing all PV parameters to approach their maximum values.

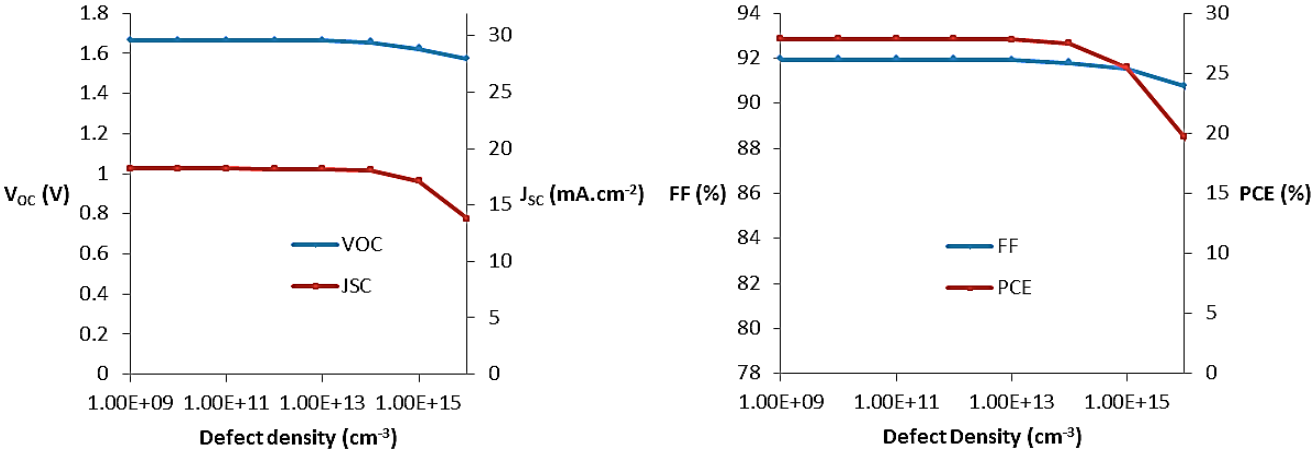

Fig. 12. Illustrates the variation of PV parameters with defect density (N_t) of second absorber layer Cs_2TiBr_6 (colour online)

Influence of HTL (NiO) thickness: An HTL principal role is to collect holes and reduce recombination at the back contact electrode and helps holes travel from the absorber layer to the rear electrode [37]. A Very large value of thickness of HTL gives holes a lengthier path to back contact electrode, which decreases the chance of electron-hole recombination. In this investigation, the thickness of an HTL was varied between 10 to 500 nm. Fig. 13 shows that adjusting the HTL thickness has no effect on the V_{oc}, J_{SC}, fill factor, or PCE. A thicker HTL has a higher series resistance, thus reducing the PCEs. To reduce the possibility of recombination, HTL must have 175 nm.

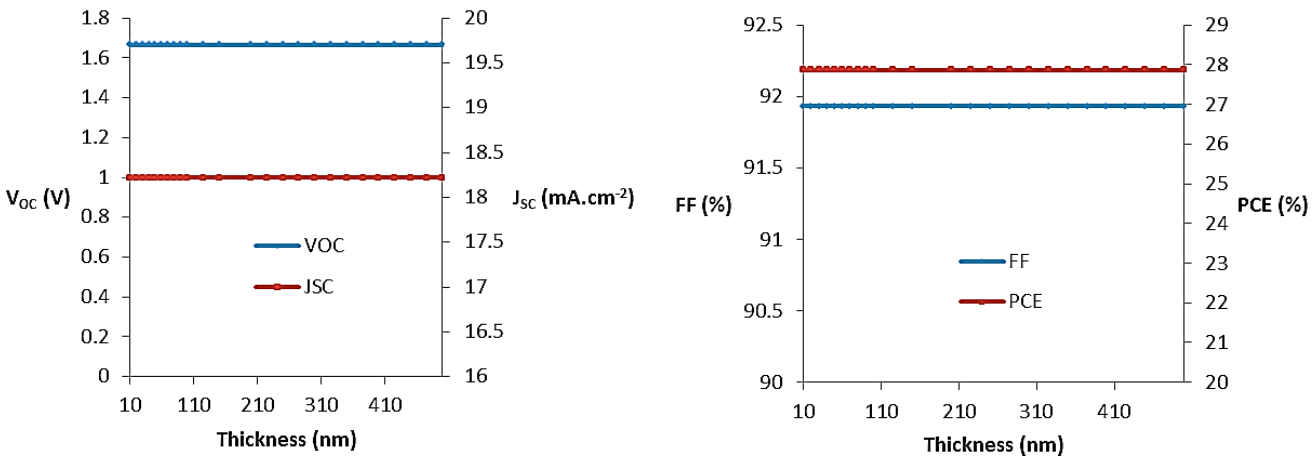

Fig. 13. Influence of HTL layer thickness on V_{oc}, J_{sc}, FF and PCE (colour online)

Influence of acceptor density (N_A) of HTL (NiO): Acceptor density was increased from 10^9 to 10^{21} cm^{-3} to improve the performance. A very minor increase in the efficiency is seen. Fig. 14 shows that the values of all parameters remained constant as the acceptor density increased. However, when the optimal value of N_A was set to 10^{16}, the highest value of PCE was discovered to be 27.86%. Higher N_A values can cause coulomb traps, leading in reduced hole mobility [38]. When the N_A of HTL is 10^{16} cm^{-3}, the suggested cell has V_{oc}, J_{sc}, FF, and PCE values of 1.6635 V, 18.22 mA/cm^2, 91.93%, and 27.86%, respectively.

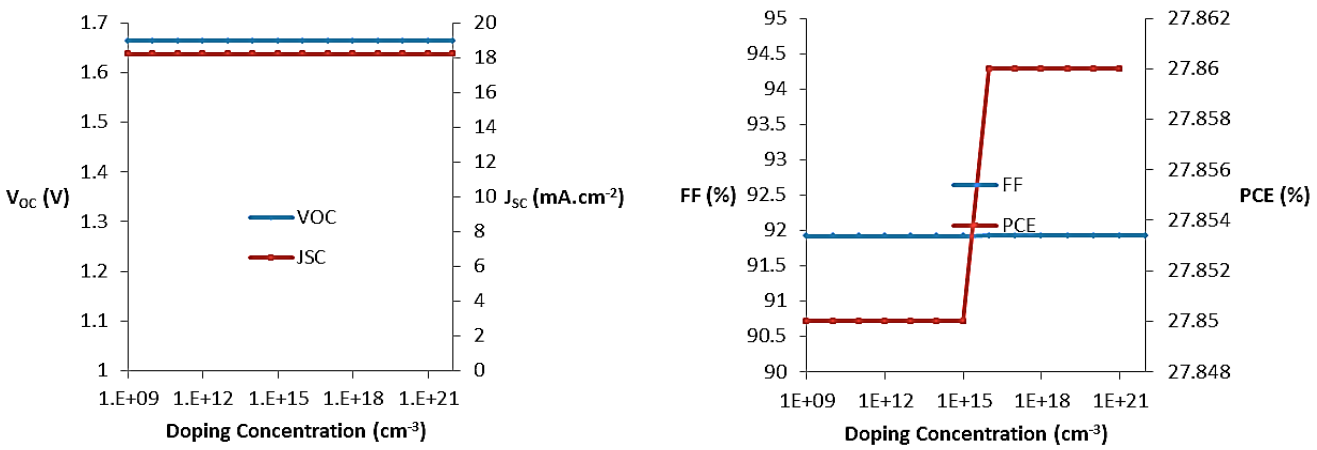

Fig. 14. Influence of acceptor density of HTL layer on V_{oc}, J_{sc}, FF and PCE (colour online)

Influence of defect density of HTL (NiO): The suggested PSC architecture's power efficiency was evaluated by changing the trap density of states (N_t) in the NiO layer from 10^9 to 10^{22} cm^{-3}. Fig. 15 depicts the effect of N_t change in the HTL (NiO) on photovoltaic characteristics. The graph indicates that V_{oc}, J_{sc}, FF, and PCE remain constant when N_t grows from 10^9 to 10^{22} cm^{-3}.

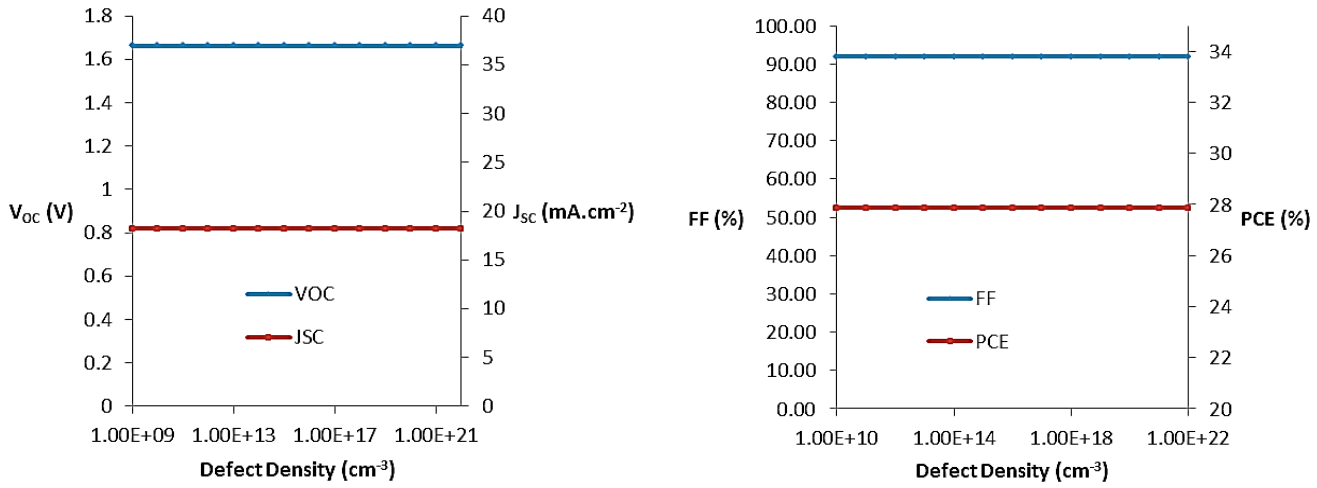

Fig. 15. Influence of defect density N_t in NiO layer on the V_{oc}, J_{sc}, FF and PCE (colour online)

Influence of temperature: Solar cell's efficiency is related to the operating temperature. Generally solar panels often work at higher temperatures, more than 300 K. In contrast, the working temperature of solar cells may change throughout production, characterization, and environmental use. As we know that ambient temperature depends on the height, time of day in a specific place, latitude and season all influence the ambient temperature. The impact of temperature on solar cell performance is examined across a temperature between 250 to 500 K. Fig. 16 depicts the PV parameters with the temperature fluctuations. The figure depicts how PV parameters vary with respect to temperature increasing up to 500 K. As the temperature rises, the V_{OC} climbs from 1.62 to 1.81 V. The PCE increases from 27.33 to 29.22% for temperature increases from 250 to 500 K. The value of J_{SC} remains constant across the full temperature range. The FF reduces from 92.80 to 88.75 mA/cm^2 as the temperature rises.

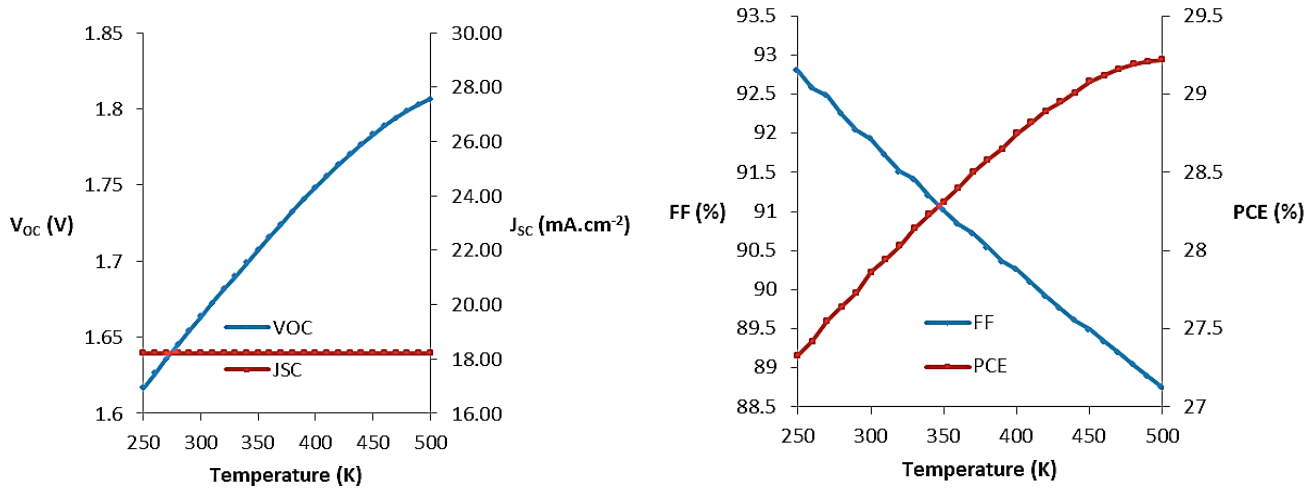

Fig. 16. Influence of temperature on V_{oc}, J_{sc}, FF and PCE (colour online)

Influence of Series Resistance (R_s): A R_s is an internal resistance of a solar cell that impedes the passage of power. Series resistance of a device affects both its fill factor and J_{sc} [39]. Bulk resistance is caused by current flow and series resistance is due to back and front contacts, interfaces etc. contact creates series resistance. Changing in R_s has an important impact on solar cell efficiency, implying that the low value of R_s produces the finest device performance. Fig. 17 displays that increasing the series resistance from 0 to 15 ohm.cm^2 reduce the PCE value from 27.86% to 23.06%. FF dropped from 91.93% to 76.08%. The value of J_{SC} remains constant across the full resistance range. A large value of R_s promotes recombination of electrons and holes by increasing the voltage drop across the solar cell, making it problematic for charge carriers to reach the back and front end. If the value of R_s is high the greater the energy loss in a solar cell [40].

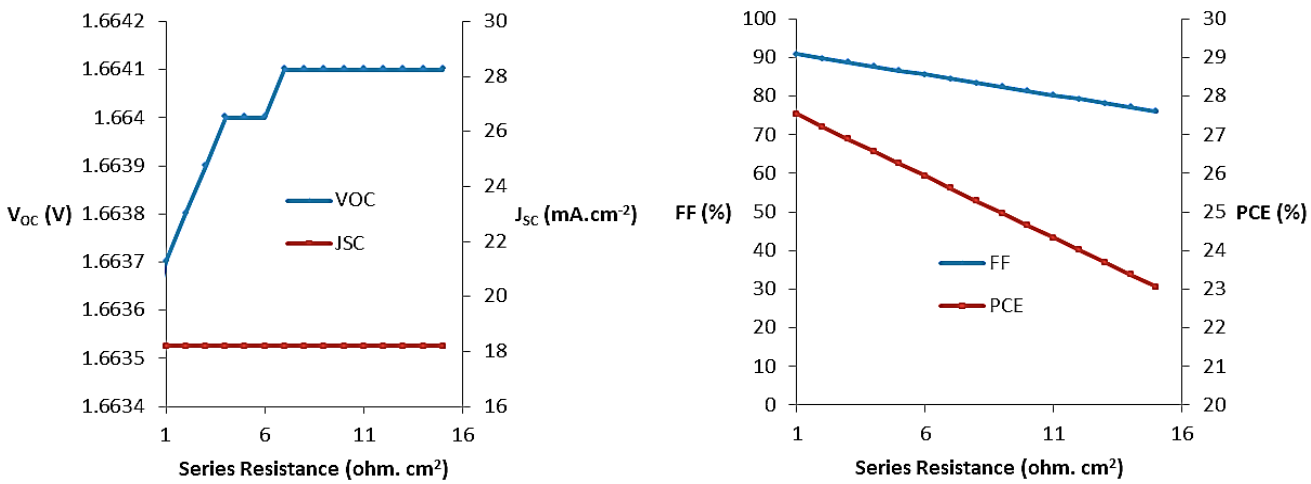

Fig. 17. Influence of series resistance on V_{oc}, J_{sc}, FF and PCE (colour online)

Influence of shunt resistance: Every electronic equipment contains some resistance. Several charge recombination mechanisms generate shunt resistance. To get greater performance, significantly higher shunt resistance is required [41]. A higher shunt resistance means that less current is dissipated along the parallel channel, which leads to a more effective solar cell. The simulation demonstrates that shunt resistance has little effect on the solar cells performance. Fig. 18, J_{SC} remains nearly constant at 18.21% while the shunt resistance is adjusted from 10^1 to 10^{15} ohm.cm^2, despite a rise in V_{OC}, FF, and PCE. As the shunt resistance increases, the V_{OC} value rises from 0.18 to 1.66 V. PCE climbed from 0.83% to 27.86%, while FF rose from 25.00% to 91.93%. This effect occurs when the shunt resistance increases, resulting in a reduction in the amount of current lost due to recombination, hence boosting FF and PCE.

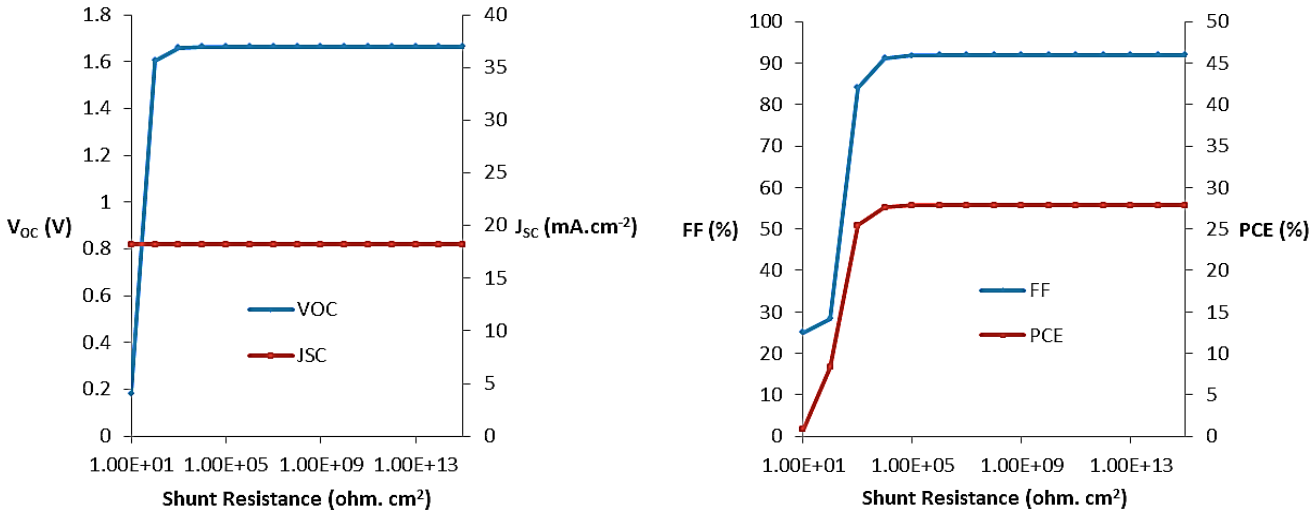

Fig. 18. Influence of shunt resistance on V_{OC}, J_{sc}, FF and PCE (colour online)

Investigation of Quantum Efficiency (QE): A PSC's QE denotes its ability to convert received photons into electrical charge carriers, specifically holes and electrons. QE is defined by the ratio of collected carriers to photons with an explicit energy that influence the solar cell [42]. Fig. 19 displays how the QE of a solar cell increases initially with wavelengths 360 nm, reaches a peak, and then drops. As a result, if the wavelength is very small or very large, the efficiency is reduced. Solar rays of the wavelengths between 330 to 670 nm are typically sufficient to release electrons from the weak bonds and generate an electric current. This occurrence is related to the material's band gap. The value of energy of photons greater than the bandgap is absorbed, but they cause generating of heat, if the energy of the photons below the bandgap is not absorbed. In this simulation, the maximum PCE is reached at a wavelength of 360 nm, as shown in Fig. 19.

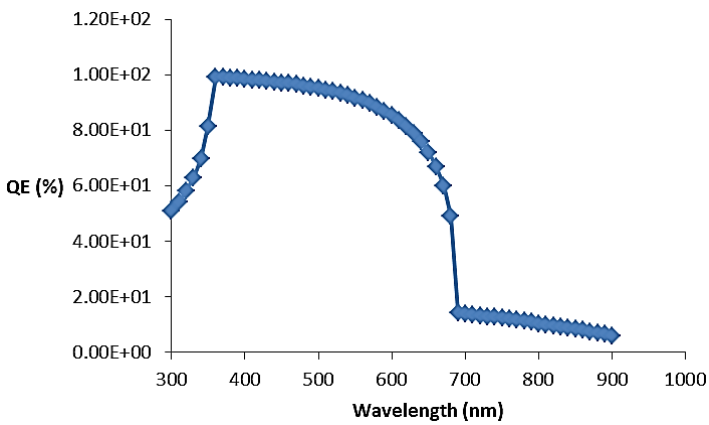

Fig. 19. The response of QE concerning incident photon wavelength for the suggested solar cell

Influence of the back contact material (work function): The material of back contact must be adjusted to increase PSC output. Its main function is to handover solar energy to an external circuit. Ohmic contact is provided by metal for connecting and must be robust and non-corrosive. Recombination rates for minority charge carriers should be lower. PSC enables the use of a variety of back contacts, such as Ag, Au, Pt and Pd. The most commonly used material for back contact is Ag, the work function of Ag is 4.5 eV. A high energy-level difference between the absorber layer and metal contact, which results in the development of Schottky junction and decreases efficiency of the device [43]. Schottky junction growth can damage the performance of a solar cell, because this junction prevents the charge flow. As a result, choosing a suitable material for back contact with a large metal work function is crucial for increasing efficiency of the solar cell. The work function's parameters vary between 4.5 to 5.2 eV. Fig. 20 displays that at work function 5.1 eV, gold (Au) has the highest PCE of 27.86%. According to this analysis, the value of work function of the material is at least 5.1 eV for optimal efficiency; lower values may result in poor performance.

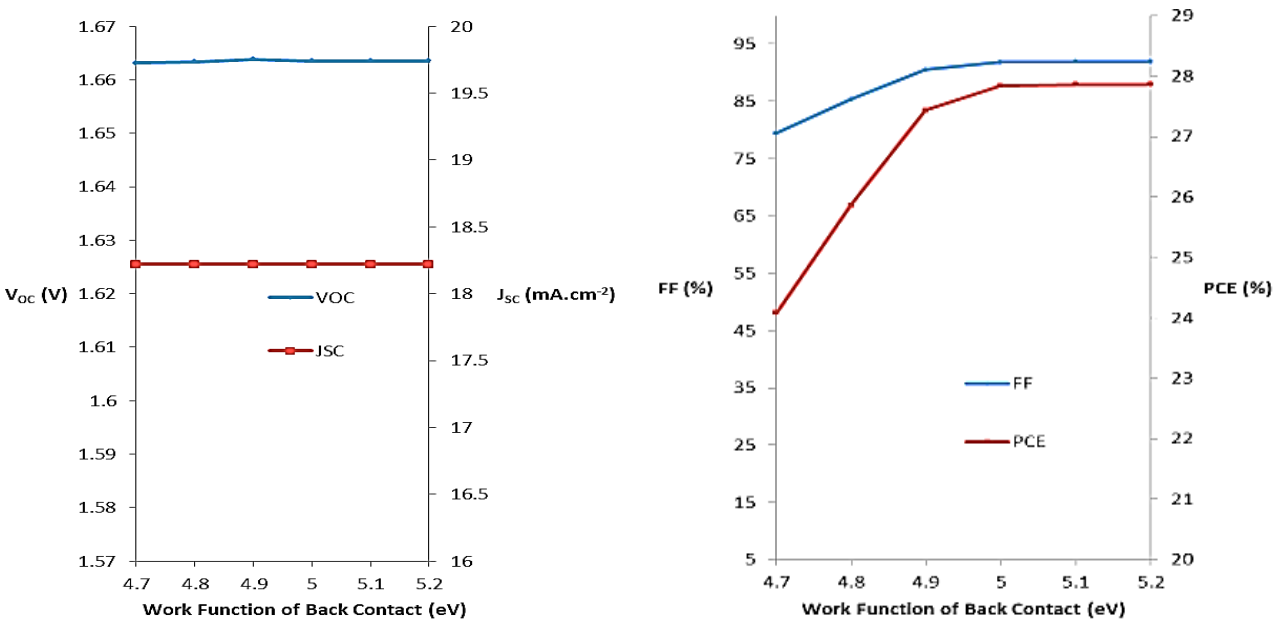

Fig. 20. Influence of back contact (work-function) on the PCE performance of the proposed structure (colour online)

4. Conclusions

In this paper we describe a Pb-free, ecologically friendly, and steady $CH_3NH_3SnBr_3$ and Cs_2TiBr_6-based inorganic PSC that uses only inorganic charge transport components. The ideal layer thinness was determined to generate a one-of-a-kind large-performance n-i-p solar cell (FTO/ZnO/$CH_3NH_3SnBr_3$/Cs_2TiBr_6/NiO/Au). In this study SCAPS-1D is used to analyse and optimize the solar cell taken for PV characterization. After optimizing all layers, a significant PCE of 27.86%, J_{SC} of 18.22 mA/cm^2, V_{oc} of 1.6635 V, and FF of 91.93% were attained. The whole world is turning to renewable energy sources. There are several chances for developing an efficient and low cost energy system. The results of the current study will not only shed light on the PV process, but will also pave the way for the development of Pb-free and highly efficient solar cells. The results of this study are likely to contribute to the progress of trustworthy and vastly efficient PSCs that do not contain lead or other dangerous substances.

Declaration of competing interest

The authors claim that they have no known competing financial interests or personal relationships that could have influenced the research provided in this paper.

Data availability: Data will be made available upon request.

Acknowledgement

We are grateful to Dr. Marc Burgelman and his colleagues (University of Gent, Belgium) for developing the SCAPS 1-D simulation software and providing free access to it.

References

[1] S. M. Najmul Hoque, B. Kumar Das, J. Renew. Sustain. Energy **5**(4), 1 (2013).
[2] A. Das, S. D. Peu, M. A. M. Akanda, A. R. M. T. Islam, Energies **16**(5), 2198 (2023).
[3] M. Kumar, A. Raj, A. Kumar, A. Anshul, Int. J. Energy Res. **46**(8), 11456 (2022).
[4] Vinod, Raj Kumar, S. K. Singh, Energy Reports, **4**, 701 (2018).
[5] I. Qasim, O. Ahmad, Z. ul Abdin, A. Rashid, M. Farooq Nasir, M. Imran Malik, M. Rashid, S. M. Hasnain, Sol. Energy **237**, 52 (2022).
[6] R. K. Shukla, A. Srivastava, S. Rani, N. Singh, V. K. Dwivedi, S. Pandey, N. Wadhwani, Integrated Ferroelectrics **240**(1), 73 (2024).
[7] R. K. Shukla, A. Srivastava, S. Rani, Nidhi Singh, Vishnu Kumar Dwivedi, Sharda Pandey, Navina Wadhwani, Journal of Optics **53**, 477 (2024).
[8] R. K. Shukla, A. Srivastava, S. Rani, N. Singh, V. K. Dwivedi, S. Pandey, N. Wadhwani, Nanosystems: Phys. Chem. Math. **15**(1), 135 (2024).
[9] Amrit Kumar Mishra, R. K. Shukla, Materials Today: Proceedings **46**, Part 6, 2288 (2021).
[10] Amrit Kumar Mishra, R. K. Shukla, Materials Today: Proceedings **29**, Part 3, 836 (2020).
[11] A. K. Mishra, R. K. Shukla, SN Appl. Sci. **2**, 321

(2020).
[12] M. Chen, M. G. Ju, A. D. Carl, Y. Zong, R. L. Grimm, J. Gu, X. C. Zeng, Y. Zhou, N. P. Padture, Joule **2**, 558 (2018).
[13] F. Igbari, Z. K. Wang, L. S. Liao, Adv. Energy Mater. **9**, 1 (2019).
[14] J. Euvrard, X. Wang, T. Li, Y. Yan, D. B. Mitzi, J. Mater. Chem. A **8**, 4049 (2020).
[15] L. Qiao, W. H. Fang, R. Long, J. Phys. Chem. Lett. **9**, 6907 (2018).
[16] W. Li, S. Zhu, Y. Zhao, Y. Qiu, J. Solid State Chem. **284**, 121213 (2020).
[17] K. Chakraborty, M. G. Choudhury, S. Paul, Sol. Energy **194**, 886 (2019).
[18] M. Ju, M. Chen, Y. Zhou, H. F. Garces, J. Dai, N. P. Padture, X. C. Zeng, ACS Energy Lett. **3**, 297 (2018).
[19] S. Mazumder, K. Senthilkumar, Sol. Energy **237**, 414 (2022).
[20] A. Das, S. D. Peu, M. A. M. Akanda, M. M. Salah, M. S. Hossain, B. K. Das, Energies **16**, 2328 (2023).
[21] Ismaila Taiwo Bello, David Omoefe Idisi, Kamaldeen Olasunkanmi Suleman, Yetunde Ajayeoba, Oluwaseun Adedokun, Ayodeji Oladiran Awodugba, Mokhotjwa Simon Dhlamini, Biointerface Res. Appl. Chem. **12**(6), 7478 (2022).
[22] J. Choi, S. Song, M. T. Ho, H. J. Snaith, T. Park, ACS Nano **10**, 6029 (2016).
[23] W. Ye, J. Xiang, F. Huang, D. Zhong, Mater. Res. Express **5**, 085506 (2018).
[24] T. Dittrich, Phys. Stat. Sol. (a). **182**, 447 (2000).
[25] H. Lu, W. Tian, B. Gu, Y. Zhu, L. Li, Small **13**, 1 (2017).
[26] A. J. Frank, N. Kopidakis, J. Van de Lagemaat, Coord. Chem. Rev. **248**, 1165 (2004).
[27] L. Huang, Z. Hu, J. Xu, X. Sun, Y. Du, J. Ni, H. Cai, Sol. Energy Mater. Sol. Cells. **149**, 1 (2016).
[28] Ardeshir Baktash, Omid Amiri, Alireza Sasani, Superlattices and Microstructures **93**, 128 (2016).
[29] R. Kour, S. Arya, S. Verma, J. Gupta, P. Bandhoria, V. Bharti, R. Datt, V. Gupta, Glob Chall. **3**(11), 1900050 (2019).
[30] Min Chen, Ming-Gang Ju, Alexander D. Carl, Xiao Cheng Zeng, Yuanyuan Zhou, Nitin P. Padture, Joule **2**, 558 (2018).
[31] K. Sobayel, M. Akhtaruzzaman, K. S. Rahman, M. T. Ferdaous, Z. A. Al-Mutairi, H. F. Alharbi, N. H. Alharthi, M. R. Karim, S. Hasmady, N. Amin, Results in Physics **12**, 1097 (2019).
[32] Q. Chen, Y. Ni, X. Dou, Y. Yoshinori, Crystals **12**(1), 68 (2022).
[33] A. Islam, N. Bin Alamgir, S. I. Chowdhury, S. M. B. Billah, Journal of Ovonic Research **18**(3), 395 (2022).
[34] A. Mohandes, M. Moradi, H. Nadgaran, Opt. Quant. Electron. **53**(6), 1 (2021).
[35] A. Hosen, S. R. Al Ahmed, J. Alloy. Compd. **909**, 164823 (2022).
[36] I. Alam, M. A. Ashraf, Energy Sources Part A Recovery, Utilization, and Environmental Effects **46**(1), 17080 (2020).
[37] B. Mahapatra, R. V. Laxmi Krishna, P. K. Patel, Opt. Commun. **504**, 127496 (2021).
[38] M. M. Salah, M. Abouelatta, A. Shaker, K. M. Hassan, A. Saeed, Semicond. Sci. Technol. **34**(11), 115009 (2019).
[39] M. Belarbi, O. Zeggai, S. Louhibi-Fasla, Materials Today: Proceedings **51**, 2115 (2022).
[40] D. Jayan, Adv. Theory Simulations **5**(5), 1 (2022).
[41] D. Saikia, J. Bera, A. Betal, S. Sahu, Opt. Mater. **123**, 111839 (2022).
[42] K. Chakraborty, M. G. Choudhury, S. Paul, Sol. Energy **194**, 886 (2019).
[43] Mamta, K. K. Maurya, V. N. Singh, Coatings **12**, 405 (2022).

*Corresponding author: krishnacdubey@gmail.com